THE IMPORTANCE OF INTERNAL CLIMATE VARIABILITY IN CLIMATE IMPACT PROJECTIONS

PUBLISHED IN PNAS AT HTTPS://DOI.ORG/10.1073/PNAS.2208095119 *

Kevin Schwarzwald
Lamont-Doherty Earth Observatory
Columbia University
Palisades, NY 10964
kevin.schwarzwald@columbia.edu

Nathan Lenssen
Lamont-Doherty Earth Observatory &
NASA Goddard Institute for Space Studies
New York, NY, 10025
n.lenssen@columbia.edu

ABSTRACT

Uncertainty in climate projections is driven by three components: scenario uncertainty, inter-model uncertainty, and internal variability. Although socioeconomic climate impact studies increasingly take into account the first two components, little attention has been paid to the role of internal variability, though underestimating this uncertainty may lead to underestimating the socioeconomic costs of climate change. Using large ensembles from seven Coupled General Circulation Models with a total of 414 model runs, we partition the climate uncertainty in classic dose-response models relating county-level corn yield, mortality, and per-capita GDP to temperature in the continental United States. The partitioning of uncertainty depends on the time frame of projection, the impact model, and the geographic region. Internal variability represents more than 50% of the total climate uncertainty in certain projections, including mortality projections for the early 21st century, though its relative influence decreases over time. We recommend including uncertainty due to internal variability for many projections of temperature-driven impacts, including early- and mid-century projections, projections in regions with high internal variability such as the Upper Midwest United States, and for impacts driven by non-linear relationships.

Keywords Climate Impacts · Climate Variability · Uncertainty Quantification · Climate Projections

Significance Statement

Statistical projections of the socioeconomic impacts of climate change are increasingly used in policy, development, and the private sector to understand and prepare for climate risks. Climate uncertainty is the dominant source of uncertainty in many of these projections. Such studies increasingly account for some sources of climate uncertainty, including differences between climate models and emissions scenarios. However, uncertainty due to internal climate variability is generally ignored. We show that internal variability substantially boosts the uncertainty by 38% on average for near-term mortality, corn yields, and GDP projections in the continental United States. Omitting uncertainty due to internal variability could lead to an underestimation of worst-case impacts and/or a misallocation of resources in climate mitigation and adaptation efforts.

1 Introduction

Studies on the socioeconomic impacts of climate change have historically underestimated climate uncertainty, leading to overconfident projections of the resulting impacts [1, 2]. Uncertainty in simulations of the future climate may arise from three major sources: 1. scenario uncertainty, representing differences in plausible future greenhouse gas

* *This Manuscript is Published as*: **Schwarzwald, K., & Lenssen, N. (2022). The importance of internal climate variability in climate impact projections. Proceedings of the National Academy of Sciences, 119(42), e2208095119. DOI: 10.1073/pnas.2208095119**

emissions trajectories, 2. (climate) model uncertainty, representing differences in model responses to the same scenario inputs, and 3. internal variability [3]. Currently, state-of-the-art analyses of future climate impacts account for scenario uncertainty by using projections from multiple future scenarios, and model uncertainty by using a multi-model ensemble of projections from coupled general circulation models (CGCMs) [1, 2, 4, 5, 6]. However, uncertainty due to internal variability is rarely taken into account despite the evidence that internal variability is an important component of total climate uncertainty for at least the first 50 years of projections [3, 7, 8, 9].

Internal variability consists of the naturally occurring variations in climate on timescales from daily weather to multidecadal processes due to interactions between various components of the Earth system. Internal variability is made up of components that are predictable, such as the El Niño-Southern Oscillation (ENSO) [10], as well as irreducible uncertainty due to the chaotic nature of the system [11]. In the continental United States (CONUS), for example, increased likelihood of droughts and higher temperatures occurs during and following El Niño events in the Pacific Northwest [12, 13], following La Niña events in the Midwest [14, 15], and during the positive phase of the Atlantic Multidecadal Oscillation [16, 17, 18]. In addition, internal variability leads to variability in trends of temperature, particularly over the northern and eastern CONUS [19, 20]. The currently best available estimates of the true internal variability of the Earth's climate system comes from multi-model ensembles of initial-condition Large Ensembles (LEs), where a CGCM is run multiple times with slight perturbations to the initial conditions to sample the distribution of its possible climate outcomes, conditioned on the same emissions scenario [21]. The LEs used in this study provide generally realistic simulations of historical temperature variability over CONUS [22].

While much of the attention in climate impacts studies is on end-of-century projections, policymakers generally respond to short-term challenges on time horizons of days to decades [23, 24], when internal variability is most prominent in projections of climate variables. It is particularly important to properly characterize the uncertainty of an impact when determining worst-case scenarios [25, 26], especially since the frequency of threshold-defined extremes often used in impact studies are more affected by changes in the variability than the mean [27, 28]. Underestimating uncertainty of an impact leads to underestimation of the socioeconomic costs of climate change [26]. Following the findings of [2] that climate model uncertainty must be accounted for to fully understand climate uncertainty in end-of-century impact projections, we suggest that a proper representation of internal variability is critical to properly represent the total climate uncertainty of shorter term projections. The recent availability of LE climate model experiments makes it possible to determine the uncertainty added by internal variability in projected socioeconomic impacts of climate change.

In this study, we quantify the climate uncertainty due to scenario, model, and internal variability uncertainties of future projections of mortality, GDP per capita, and corn yields. Each of these impacts are assumed to be driven by temperature changes at the county level over the Continental United States (CONUS). By comparing the relative magnitude of variance contributed by each source of uncertainty, we identify the conditions where the inclusion of internal variability is critical to accurately representing the uncertainty of a future climate impact.

2 Partitioning climate uncertainty in climate impact projections

In this study, we quantify and partition the climate uncertainty in socioeconomic studies that use statistical models to link observed weather and climate to an impact of interest; that is, we determine what share of their climate uncertainty comes from scenario, model, or internal sources. In such impact studies, the relationship between an observed or projected climate variable (Figures 1d.,h.) and socioeconomic outcomes (Figures 1a.-c.) is represented through a dose-response function (Figures 1e.-g.), estimated through the historical relationship between a climate variable and a socioeconomic impact [4]. With the relationship between climate and an impact established through the dose-response function, future impacts are determined by: (1) estimating the projected change in climate using CGCM simulations, and (2) using the dose-response function to calculate the future change in the impact of interest. Other approaches to modeling future climate impacts, such as process-based or top-down models, may use climate projections at different stages of the projection of damages [29]; climate uncertainty may therefore propagate differently than through dose-response functions. In process-based crop models in particular, recent studies have shown substantial influences of internal variability in projections of future crop yields in Sub-Saharan Africa [30] and Canada [31].

We investigate the importance of internal variability by revisiting three classic dose-response functions. We selected studies with three different common shapes of dose-response functions, providing a broad survey of the possible effects of internal variability on impact uncertainty. For ease of comparison, we chose dose-response functions that all relate an impact variable to temperature over CONUS, calculated at the county-level. While the current state-of-the-art dose-response functions often use multiple climate variables as inputs and evolve in time to account for changes in adaptation [4, 6], focusing on simple, stationary functions of temperature applied to a constant population distribution allows for clear interpretation of the decomposed climate uncertainty. Specifically, we selected the U-shaped relationship

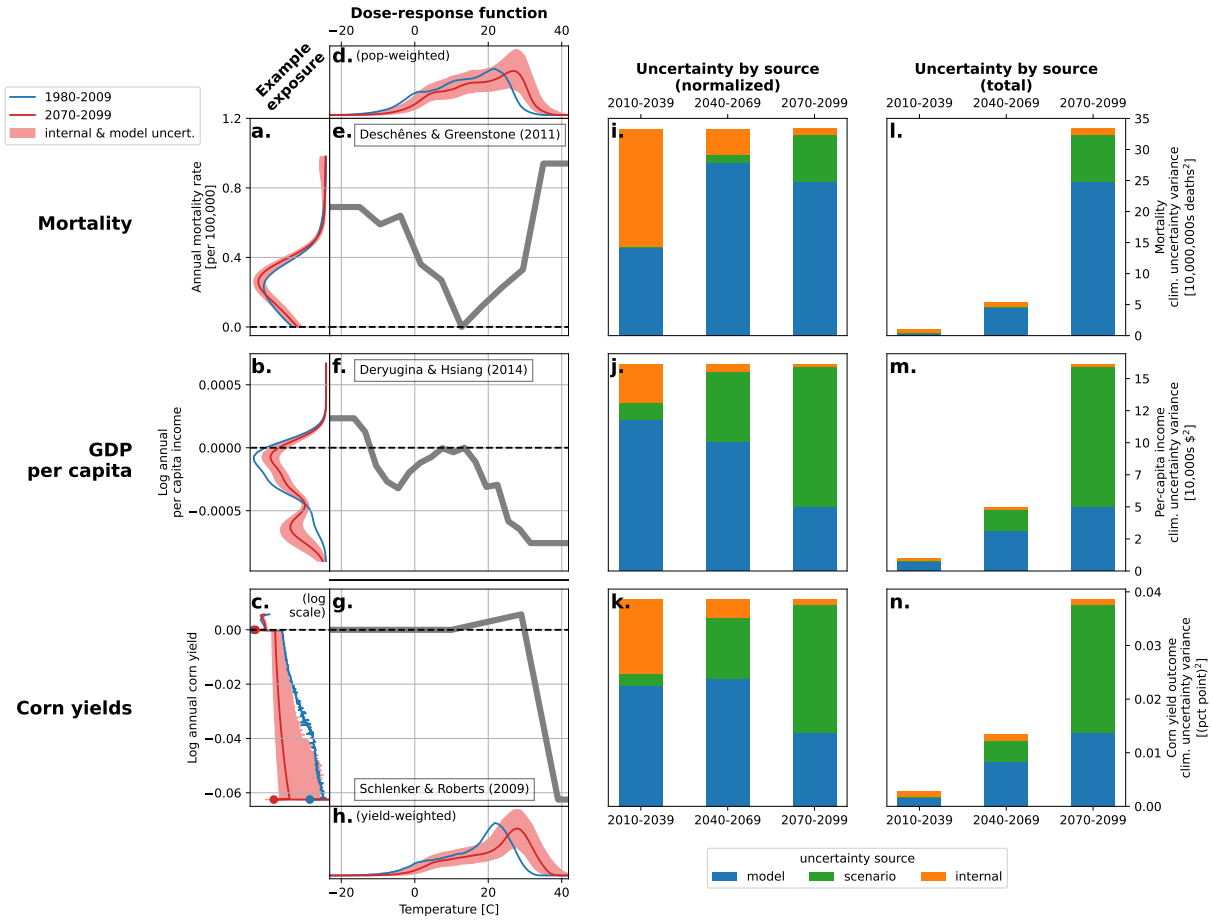

Figure 1: Climate uncertainty in the projections of climate impacts. Dose response functions (e.-g.) relate a variable of societal interest to historical climate distributions (d., h., showing the 1980-2009 county level population-weighted and corn yield-weighted temperature distributions, respectively), thereby estimating an exposure to the impact (a.-c., blue line). Future projections of impact variables are constructed by inputting future temperature projections (d., h. red line, representing the average distribution across all LE runs), leading to exposure to a future impact distribution (a.-c., red line, representing the average impact across all LE runs). However, future temperatures are uncertain (d., h., red filled region showing range of future temperature distributions across all runs of all LEs, representing internal and model uncertainty), leading to uncertainty in impacts projections (a.-c., red filled region). This climate uncertainty can be decomposed into contributions from internal (i.-n., orange), scenario (green), and model (blue) uncertainty, which are shown as relative (i.-k., values in Table S1) and absolute variances (l.-n., values in Table S2). Internal variability is substantial in the early 21st century (i.-k., leftmost column), especially for projections of mortality and corn yields, while model (for mortality) or scenario (for GDP per capita and corn yields) uncertainty dominates by the end of century (i.-k., rightmost column). Internal variability remains roughly constant in absolute terms throughout the century, while model and scenario uncertainty increase over time (l.-n.).

between mortality and temperature of [32] (Figure 1e.), the roughly decreasing relationship between GDP per capita and temperature of [33] (Figure 1f.), and the the cutoff-style relationship between corn yield and temperature, where yield rapidly decreases with temperature after a threshold temperature is exceeded of [34] (Figure 1g.).

Using the LE multi-model archive, we construct early (2010-2039), mid (2040-2069), and late (2070-2099) 21st century projections of daily temperature by adding the relative change in monthly mean temperature from the LE simulations to 30 years of daily ERA-INTERIM reanalysis data (1980-2009). This projection method accounts for annual mean temperature change as well as any changes to the seasonal cycle, but not changes in the distribution of daily temperature within a month [35, 36]. The changes to the daily temperature distribution are not explored here as not all LEs in the study provide daily temperature projections. Incorporating the daily temperature distribution changes will likely not

affect the CONUS results presented here as internal variability is dominated by longer-term trend uncertainty [20]. However, these changes may be more important to include in regions of lower trend internal variability.

To construct impact projections of mortality, per capita GDP, and corn yield changes, we input the differences between future temperature projections and historical temperature records into the dose-response functions of [32, 33, 34], respectively. A CONUS-wide impact is calculated for each ensemble member by the weighted average over all counties where the weighting is by county population for mortality and per capita GDP and by historical average corn yield for corn yield. Internal variability is estimated as the mean of the impact variances for each model, while the inter-model uncertainty is estimated as the variance of the ensemble means of each calculated impact.

Since most of the models in the LE archive were only run using a single future greenhouse gas scenario – the RCP8.5 "high baseline emissions" scenario [37] – another method must be used to determine the scenario uncertainty of the projected impacts. Following current best practices in large ensemble studies, we estimate the scenario uncertainty as the variance across scenarios of the multi-model mean across models from the 5th Phase of the Coupled Model Intercomparison Project (CMIP5), using all CMIP5 models which have data for the RCP2.6, RCP4.5, RCP6.0, and RCP8.5 scenarios [38]. Following [39], we alternatively calculate scenario uncertainty using MPI-ESM, the only LE in the sample with data from RCP2.6 and RCP4.5 in addition to RCP8.5 and the LE best replicating CONUS internal variability [40], and highlight results where relevant.

3 Results

Our projections of mortality, GDP, and corn yield changes due to climate change are similar in magnitude to the original estimates of [32, 33, 34]. Each of these studies originally underestimated the full uncertainty in their projections; [32] by using only one run from one model and therefore ignoring all three sources of uncertainty, [34] by incorporating scenario but not model or internal uncertainty, and [33] by incorporating model but not scenario or internal uncertainty.

The total climate uncertainty in each aggregated impact over CONUS grows throughout the 21st century (Figures 1l.-n.), as would be expected as greenhouse gas emissions scenarios diverge, increasing scenario uncertainty, and growing differences in inputs from historical baselines enhance the differentiation between models, increasing model uncertainty. We see an increase in the variance of climate uncertainty from early to late 21st century by a factor of 35 for mortality, 16 for GDP, and 14 for corn yield. This growth in uncertainty is largely due to increases in model and scenario uncertainties, with uncertainty due to internal variability remaining approximately constant over time for projections of each of the three impacts.

Internal variability is particularly important in projections of strongly nonlinear impacts over 2010-2039 such as mortality (57% of climate uncertainty, Figure 1i. and Table S1 top segment) and corn yields (37% of climate uncertainty, Figure 1k. and Table S1 bottom segment). Even for a relatively linear dose-response function such as GDP, internal variability plays a considerable role in early-century projections, underscoring the need to account for internal variability for projections made on scales of years to a few decades. Conditioned on the RCP8.5 scenario that forced the LE runs, internal variability continues to make up 6-13% of the joint model-internal uncertainty by mid-century and 4-7% by end-of-century.

The climate uncertainty partitioning is different for each of the three impact projections. By the end of the 21st century, impact projection uncertainty is largely driven by model and scenario uncertainty. The relative weight of the three sources of uncertainty in impact projections is determined by the shape of the dose-response function, despite uncertainty in mean CONUS temperature change projections being dominated by scenario uncertainty (Figure S1). The mortality dose-response function, which features a turning point towards the middle of the historical temperature distribution (Figure 1e), is particularly affected by model uncertainty well into the 21st century. Small differences in exposure to temperatures on either side of the turning point in any scenario can have large consequences in the CONUS average for the balance between counties with expected increases and those with expected decreases in mortality.

The climate uncertainty partitioning of each impact projection is different from the climate uncertainty partitioning in mean temperature (Figure S1). In particular, uncertainty due to internal variability is greater in each of the three impact projections than in temperature, demonstrating how a small contribution of internal variability to total climate variability for raw temperature does not imply that internal variability can be ignored in an impact projection that depends on temperature.

The projection of climate impacts interacts with internal variability in complex and often non-intuitive ways. This is illustrated through the ensemble members of the CESM1-CAM5 model that project the highest and lowest mortality change between the historical and mid-century time periods (Figure 2). Both ensemble members have similar changes in CONUS mean temperature (Figure 2a.). However, geographic (Figures 2c.,d.) and seasonal (Figure S2) variability in trends produce nearly opposite patterns of changes in mortality rates compared to the ensemble mean change (Figures

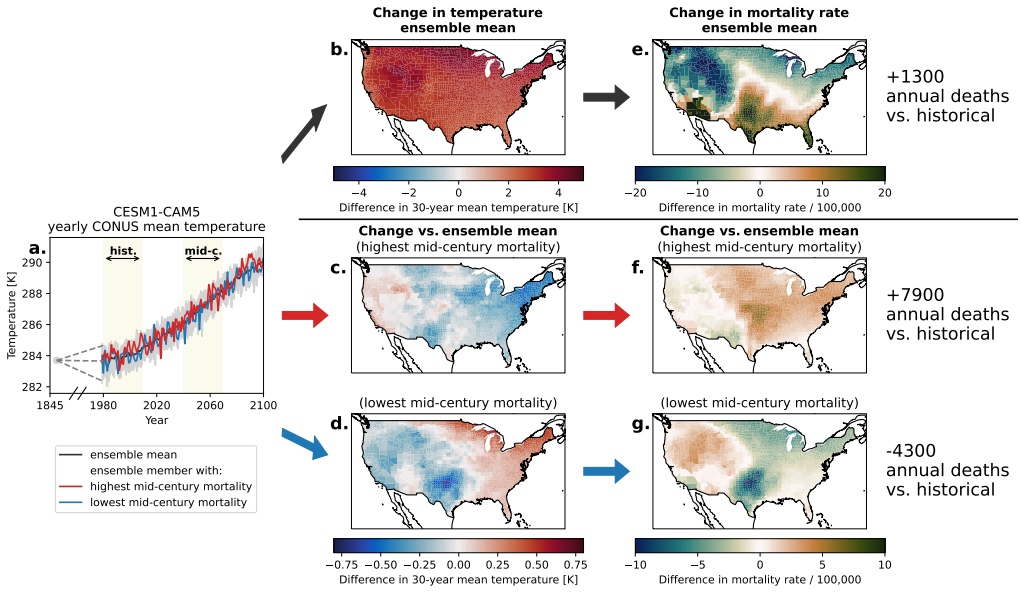

Figure 2: Example of how internal uncertainty propagates through projections of changes in heat-related mortality CESM1-CAM5. This figure shows the ensemble mean change in temperature (black line in a. and panel b.) and mortality rate (e.; 1300 additional annual deaths vs. historical average), the same for the ensemble member projecting the highest mortality in mid-century (7900 additional annual deaths vs. historical average; red in a. and middle row), and the same for the ensemble member projecting the lowest mortality in mid-century (4300 fewer annual deaths vs. historical average; blue in a. and bottom row). Note the different ranges on the colorbar between the ensemble mean (top) and the relative changes (middle and bottom). Variability in trends is produced by both seasonal (Figure S2) and geographic (c.-d., S3) differences.

2f.,g.), with the greatest variability found in the Upper Midwest and Texas in this model (Figure S3). The ensemble member with the highest mortality change has particularly high increases in mortality rates in eastern CONUS while the member with the lowest change projects particularly low mid-century mortality rates in south-central and eastern CONUS. When accounting for the spatial distribution of population, we project 7,900 additional annual heat-related deaths in the highest mortality ensemble member by mid-century compared to the 1980-2009 average, and 4,300 *fewer* deaths in the ensemble member with lowest projected mortality. These represent an increase of 0.3% and a decrease of 0.2%, respectively, relative to 2.7 million total deaths in CONUS in 2015 [41]. Thus, the dominant sources of climate uncertainty in a projected impact depend on both the dominant source of climate uncertainty in each county-level impact as well as the spatial distribution of the population affected. Critically, this population distribution may not overlap with the areas of greatest climate uncertainty.

A large portion of model uncertainty, particularly in projections of mortality, is due to the outlier GFDL-CM3 model (Figures 3, S4), which projects particularly strong warming during the summer over much of CONUS. That is, GFDL-CM3 projects a substantial shift in the shape of the average seasonal cycle not found in other models (Figures S5, S6). These differences are less pronounced when mean temperature is weighted by historical corn yields, explaining the lower discrepancy between variability calculations with or without GFDL-CM3 in corn yield projections (Figures S4, S5). Though the global warming response to increased greenhouse gas concentrations in GFDL-CM3 falls within the limit of plausible climate sensitivities based on our current understanding of historical and paleoclimate records and emergent constraints [42], many aspects of model's performance over CONUS have not yet been evaluated. Removing GFDL-CM3 from the variability partitioning calculation increases the relative importance of internal variability in all three impact projections (Figure S7g.-i.). Further subsetting to the four models that best replicate the internal and forced response over North America (MPI-ESM, CanESM2, CESM1-CAM5, and GFDL-ESM2M [40]), does not substantially change the absolute magnitude of internal variability, but further decreases the relative importance of model uncertainty (Figure S7j.-l.), as would be expected from selecting models based on a common, observational target.

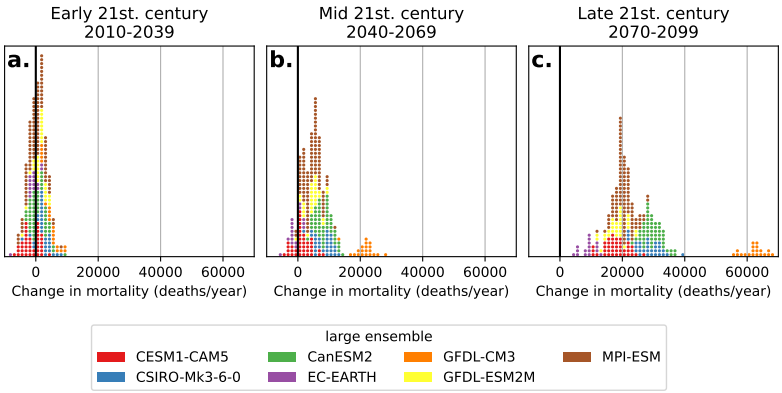

Figure 3: Histogram of projections of heat-related mortality changes in CONUS across LEs by the (a.) early (2010-2039), (b.) middle (2040-2069), and (c.) late (2070-2099) 21st century, compared to the 1980-2009 period. Each dot represents a projection constructed from a single LE run, colored by model. Figure shows internal variability as the spread of dots of a single color, and intermodel variability as the spread between dots of different colors. Internal variability dominates at the start of the century, i.e., the spread of dots of a given color is similar to the spread of all runs (a.), while intermodel variability dominates by the end of the century. GFDL-CM3 is an outlier due to its unique shifts in its seasonal cycle in CONUS (Figures S5,S6).

The partitioning of climate uncertainty in each impact is robust to ensemble size as shown by repeating the calculation with 16 ensemble members per model, the number of runs in the smallest ensemble (Figure S7d.-f.). This suggests that 16 ensemble members are sufficient to sample the internal variability of relevance to these dose-response functions over CONUS. Similar results have been found in projections of trends of climate variables alone; [43] for example showed that 10 ensemble members may be enough to sample the spread of mean temperatures in the middle of the CONUS region. Note that substantially more ensemble members may be needed to fully sample internal variability in regions with larger and more complex patterns of internal variability.

Since most LEs in the sample only have output from the RCP8.5 scenario, scenario uncertainty is calculated using output from CMIP5 models [38]. However, scenario uncertainty is similar when calculated using MPI-ESM, the one LE in the sample with data from multiple scenarios (Figure S2 m.-o.).

Decomposing the projected mortality uncertainty spatially shows that internal variability is more substantial in certain regions of CONUS (Figures 4a.-c. and Figure S8). Notably, internal variability accounts for around 50% of the total climate uncertainty in the mid-century projection of mortality in the northern Midwest, a region known to exhibit large uncertainty due to internal variability in temperature trends [20]. The GDP (Figures 4d.-f. and Figure S9) and corn yield (Figures 4g.-i. and Figure S10) impacts show similar spatial inhomogeneities, but with less contribution from internal variability, as expected from their CONUS-average values. In general, regional differences in variability may be masked by spatial averages of impact estimates.

The spatial distribution of uncertainty also highlights why scenario uncertainty is less important in end-of-century projections of mortality than in projections of corn yields or GDP per capita. The dose-response function has a turning point close to the middle of the temperature distribution and the various scenarios are approximately centered on this turning point. As a result, in each projection scenario, some counties are expected to experience decreases in mortality due to a reduction in exposure to extreme cold that outweighs the increase in exposure to extreme heat, and vice-versa. The geographic area where both effects cancel each other out is visible as the counties with nearly no relative contribution to uncertainty from scenario uncertainty in Figure 4c.

We note that the dose-response functions themselves have uncertainty arising from drawing a statistical relationship between climate and socioeconomic outcome. Each of the three dose-response functions used in this study were published with statistical uncertainty estimates. As this study focuses on the role of internal variability in total climate uncertainty, the additional uncertainty added by the dose-response uncertainty was not investigated. However, climate uncertainty tends to be a substantial, if not the dominant source of uncertainty in many impacts projections (see e.g., [2] or Figure S7 in [5]).

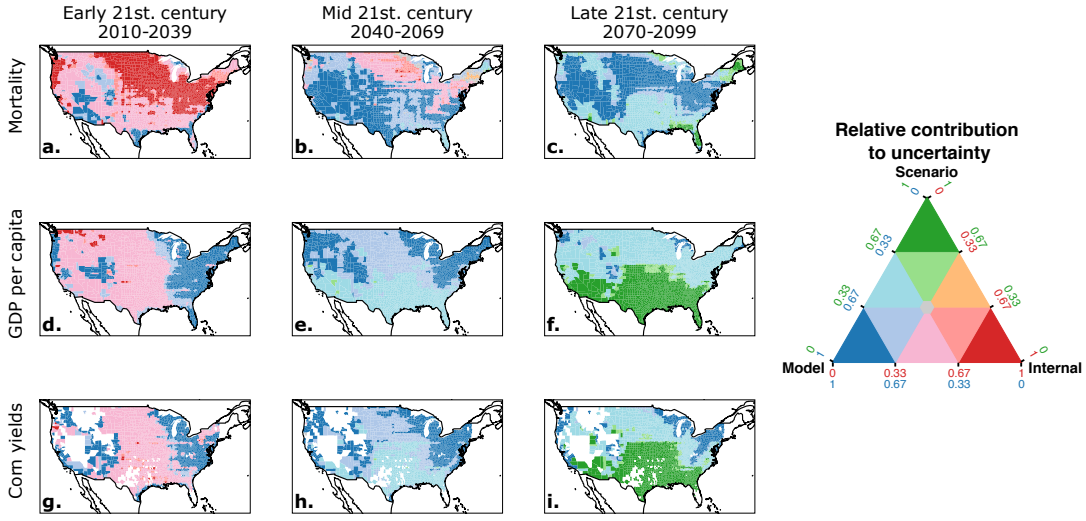

Figure 4: A spatial decomposition of the three sources of climate uncertainty on mortality (top), per capita GDP (middle), and corn yields (bottom) impacts for 30-year periods in early (left), mid (center), and late (right) 21st century projections. The band of counties in end-of-century mortality projections dominated by model uncertainty reflect the turning point in the dose-response function of [32]; in counties north of this band, mortality is expected to decrease, while in counties south of this strip, mortality is expected to increase. Blank counties in the bottom row had no corn production reported in the NASS database from 1979-2010. See Figures S8-10 for maps showing the magnitude of each individual source of uncertainty.

4 Discussion

We have investigated the sources of climate uncertainty in projections of mortality, GDP per capita, and corn yields over CONUS using dose-response functions from the literature, and have found that previously unaccounted for internal variability can have a substantial influence on uncertainty in future climate impact projections. While results will differ based on timescale, shape of dose-response function, and location as shown, internal variability is particularly impactful in 1. Early- to mid-century impacts 2. Impacts with dose-response functions that exhibit turning points close to the center of the historical climate distribution 3. Impact studies in regions where natural variability in historical climate patterns or trends is a bigger component of the climate signal.

We have focused specifically on climate impact studies based on the estimation of dose response functions using historical data. Internal variability is likely to also be relevant to other methods of estimating the impacts of climate change, such as process-based models, IAMs, or top-down approaches, though given their different relationship with climate inputs, more research may be needed to fully understand how climate uncertainty propagates through their impact projection processes. Furthermore, this study is limited to simple functions of temperature in CONUS. Studies focusing on other regions or the impacts of different climate variables may be affected by a different partitioning of the three sources of climate uncertainty. Other regions may see a lower contribution from internal variability as CONUS is a known region of high internal variability in temperature [20, 21]. Uncertainty in precipitation trends are known to depend more on internal variability than temperature trends in many regions of the world [44, 45]; future studies should investigate the relative role internal variability plays in these other domains as well. The impact projections that we investigated also do not account for future changes in adaptation behavior or geographical shifts in population or cropped areas; climate uncertainty would interact with these changes in complex ways, since future changes in distributions of impact variability depend in turn on future climate states.

In the three projections evaluated here, the relative contribution of internal variability to impact climate uncertainty is generally greater than the corresponding relative contribution of internal variability to uncertainty in temperature.

Therefore, decompositions of climate uncertainty in mean temperature and precipitation projections such as [3, 38] may not be sufficient to justify excluding climate variability uncertainty from impact projection studies.

Uncertainty in the future impacts of climate change are not necessarily reduced by CGCM improvements alone [3]. For projections on near-term, decision-relevant timescales, that involve climate impacts with strongly non-linear relationships with climate variables, or impacts in parts of the world with significant present-day climate variability, the most important source of uncertainty may be unrelated to climate change, but instead arise from the internal, existing variability of the climate system. Conversely, for end-of-century projections, involving variables with fairly linear relationships with climate variables, and for impacts in parts of the world with low existing variability, the most important source of uncertainty may be scenario uncertainty, i.e., uncertainties in human collective decision-making.

Generally, impact projection studies should account for uncertainty due to internal variability when at least one of the three conditions above is met. Including internal variability is increasingly feasible with the larger size of CMIP6 historical and projection ensembles, in addition to the multi-model large ensemble archive used in this study. However, the additional computational and software development costs to include internal variability can be substantial, which may be inefficient if the climate uncertainty of an impact is dominated by model and/or scenario uncertainty at the timescales or location of interest. By including all relevant sources of climate uncertainty, impact projections better represent worst-case outcomes that can be prepared for or prevented through climate adaptation and mitigation.

5 Methods

5.1 Climate data

5.1.1 Multi-Model LE Archive

We use all seven models that provide output from 1950-2100 and contain ensembles of at least 16 members from the multi-model large ensemble archive (Table S3 and Table 1 of [21]). Each model is forced with historical forcings from 1950-2005, and RCP8.5 forcings from 2006-2100. We use monthly near-surface air temperature from each ensemble member of each model. We use monthly data, since not all models saved output at a higher temporal resolution.

5.1.2 CMIP5 models

To characterize scenario uncertainty, we use 14 models from the 5th edition of the Coupled Model Intercomparison Project (CMIP5 [46], Table S4). We use every model that had available near-surface monthly temperature output for all four 21st-century scenarios (RCP2.6, RCP4.5, RCP6.0, and RCP8.5 [37]). Note that this selection of models includes several which have LE configurations that are included in this study (GFDL-CM3, GFDL-ESM2M, CSIRO Mk3.6.0).

5.1.3 Historical climate data

We use daily mean, maximum, and minimum near-surface air temperature data from ERA-INTERIM [47] from 1980 to 2009 to characterise historical temperature over CONUS. Mean temperature is used for calculating mortality and GDP impacts and maximum and minimum temperature are used to calculate corn yield impacts.

5.2 Building climate projections

We develop a series of climate projections for each climate model and ensemble member to quantify the uncertainty in future projections of climate impacts. Daily temperature projections are made with the “delta method" [48, 49] (sometimes also known as the “change factor method"), which assumes that model *changes* are less biased in absolute terms than model mean states. All calculations occur for each pixel separately. First, 1980-2009 ERA-INTERIM daily temperature at all pixels covering CONUS are regridded to each model's grid to create T_i^{ERA}, the base period temperature time series for day d in month m for a particular model. Then, temperature projections T_f are constructed as follows for each future time period $f = [2010, 2039],\ [2040, 2069],\ [2070, 2099]$:

$$T_f(d,m) = T_i^{ERA}(d,m) + \left(\overline{T}_f^{mod}(m) - \overline{T}_i^{mod}(m)\right) \tag{1}$$

Where $\overline{T}_i^{mod}(m)$ is a given model run's 1980-2009 average temperature for month m across all years and $\overline{T}_f^{mod}(m)$ is a given model's average temperature for month m across all years in time period f. Then T_f is a 30-year time series of daily temperature, projected from the historical time period by changes in monthly average temperatures taken from a particular run from an LE or a CMIP5 model. These projections are repeated for each run in each LE and for each CMIP5 model, creating an ensemble of future temperature projections over CONUS.

Using the method above, we create future projections of the mean, minimum, and maximum daily near-surface air temperature. Since most LEs used in this study did not save minimum or maximum air temperature, we project both of these variables by the change in the mean daily temperature.

This projection method accounts for annual mean temperature change as well as any changes to the seasonal cycle. However, it ignores well-known changes in the shape of the daily temperature distributions [35, 36], which are not considered here as many of the CGCM LEs used in this study only published monthly data.

5.3 Dose-Response Functions

The dose-response functions used are the estimates as given in the studies on mortality [32], GDP per capita [33], and corn yield [34]. We use the methodologies of each original dose-response function project to convert differences in temperature time series into projections of climate impacts; a summary of these methodologies is reproduced here for convenience.

Mortality The mortality dose-response function of [32] is based on 10°F - wide temperature bins from less than 10°F to more than 90°F. For each pixel, the change in the number of days per year in each temperature bin between the historical and a given future time period is dotted into the dose-response function to get the change in annual mortality rate / 100,000. After this change in mortality rate is aggregated to the county level, the total CONUS mortality change is calculated as the sum across counties of the product of the change in mortality rate and the population in each county. We use the total population in each county in 2015 from the SEER database [50].

GDP per capita The GDP per capita dose-response of [33] is based on 3°C - wide temperature bins from less than -15°C to more than 30°C. For each pixel, the change in the number of days per year in each temperature bin between the historical and a given future time period is dotted into the dose-response function to get the log change in annual GDP per capita. After this change is aggregated to the county level, the total CONUS GDP per capita change is calculated as the population-weighted average of each county's GDP change across all counties.

We use 2015 GDP per capita for counties from the Bureau of Economic Analysis's County-Level GDP estimates [51].

We only use the effect of the current year in [33] (i.e., the terms involving $\tilde{T}_{it}^{m}$ in their equation 9), and ignore the effect of the prior year, which the authors conclude are statistically insignificant.

Corn yields We use the piece-wise linear formulation of the corn yield-temperature dose response function of [34] (e.g., the red line in their Figure 1A). As in that study, we model the progression of daily temperature by fitting a sinusoidal between the minimum and maximum temperature (discretized using 15 points per day). The impact calculation is similar to that of mortality and GDP above, though additionally scaled by the number of points used to discretize daily temperature distributions.

We use corn yields from the USDA's National Agricultural Statistical Survey's county-level corn yields database [52], and take the average corn yield per county from 1979-2010.

We report the average change in county-level corn yields for CONUS by aggregating across counties with corn production in the sample, and weighting by this county-level corn production. We follow [34] and report results in percent change over the historical period.

5.4 Projecting impacts

Each impact projection is calculated at the pixel level before aggregating to counties; e.g., we create projections of changes in mortality rate for each pixel. This is done to minimize distortions that may occur upon geographical aggregation and to preserve the within-county temperature variation.

We then aggregate changes in mortality rate, GDP per capita, and corn yield to the county level, by for each county area-averaging all pixels that overlap with the given county, weighted by the area overlapping between each pixel and the county. CONUS-wide estimates of changes in mortality, GDP per capita, and corn yields are then calculated by aggregating results across all counties, weighting by county-level population (for mortality, GDP per capita) or corn yields.

A single estimate for the change in an impact variable is calculated for each run in each model for the entire CONUS by aggregating county-level results.

5.5 Partitioning climate uncertainty in impact projections

Climate uncertainty is calculated as the variance across estimates for total CONUS mortality, GDP per capita, and corn yield changes, following the partitioning methodology of [3]. Estimates are calculated for each run in each large ensemble (RCP8.5), and for each CMIP5 model in the sample for each scenario (RCP2.6, RCP4.5, RCP6.0, RCP8.5).

Internal uncertainty Internal uncertainty is calculated as the mean across LEs of each LE's variance of outcomes across runs.

Model uncertainty Model uncertainty is calculated as the variance across LEs of each LE's mean of outcomes across runs.

Scenario uncertainty Since most LEs were only run on one scenario due to computational constraints, we follow [3, 38] and estimate scenario uncertainty using a range of CMIP5 models. Many of the LEs used in this sample are versions of the models submitted to the CMIP5 project; CMIP5 models therefore provide a reasonable estimate of the scenario uncertainty that LEs would show. Scenario uncertainty is calculated as the variance across scenarios of the mean outcome across CMIP5 models for each scenario. In Figure S7m.-o., we alternatively show scenario uncertainty calculated using the MPI-ESM LE, which had saved output for the RCP2.6 and RCP4.5 scenarios in addition to RCP8.5, as was done by e.g. [39]. In this case, scenario uncertainty is calculated as the variance across scenarios of the mean outcome across MPI-ESM ensemble members.

Data availability

Source code and raw data has been deposited to Mendeley Data (`https://data.mendeley.com/datasets/48m4scp8jx/2`). The most up-to-date code is available on GitHub at `https://github.com/ks905383/iv_impacts`.

Acknowledgments

We thank the editor and two anonymous reviewers for their constructive comments that improved the presentation of this work. We are grateful for thoughtful comments from James Rising, Mingfang Ting, Kate Marvel, Tom Bearpark, Corey Lesk, Gernot Wagner, and the Large Ensemble community. We would also like to thank the US CLIVAR Working Group on Large Ensembles for coordinating the multi-model large ensemble experiment and making the data public.

References

[1] Maximilian Auffhammer, Solomon M. Hsiang, Wolfram Schlenker, and Adam Sobel. Using Weather Data and Climate Model Output in Economic Analyses of Climate Change. *Review of Environmental Economics and Policy*, 7(2):181–198, July 2013.

[2] Marshall Burke, John Dykema, David B. Lobell, Edward Miguel, and Shanker Satyanath. Incorporating Climate Uncertainty into Estimates of Climate Change Impacts. *The Review of Economics and Statistics*, 97(2):461–471, May 2015.

[3] Ed Hawkins and Rowan Sutton. The Potential to Narrow Uncertainty in Regional Climate Predictions. *Bulletin of the American Meteorological Society*, 90(8):1095–1108, August 2009.

[4] Tamma A. Carleton and Solomon M. Hsiang. Social and economic impacts of climate. *Science*, 353(6304):aad9837, 2016.

[5] Solomon Hsiang, Robert Kopp, Amir Jina, James Rising, Michael Delgado, Shashank Mohan, D. J. Rasmussen, Robert Muir-Wood, Paul Wilson, Michael Oppenheimer, Kate Larsen, and Trevor Houser. Estimating economic damage from climate change in the United States. *Science*, 356(6345):1362–1369, June 2017.

[6] Delavane Diaz and Frances Moore. Quantifying the economic risks of climate change. *Nature Climate Change*, 7(11):774–782, November 2017.

[7] Clara Deser, Reto Knutti, Susan Solomon, and Adam S. Phillips. Communication of the role of natural variability in future North American climate. *Nature Climate Change*, 2(11):775–779, November 2012.

[8] Clara Deser, Adam Phillips, Vincent Bourdette, and Haiyan Teng. Uncertainty in climate change projections: The role of internal variability. *Climate Dynamics*, 38(3):527–546, February 2012.

[9] Daniel Hillel and Cynthia Rosenzweig. *Handbook of Climate Change and Agroecosystems: Global and Regional Aspects and Implications*. World Scientific, 2013.

[10] Michelle L. L'Heureux, Aaron F. Z. Levine, Matthew Newman, Catherine Ganter, Jing-Jia Luo, Michael K. Tippett, and Timothy N. Stockdale. ENSO Prediction. In Michael J. McPhaden, Agus Santoso, and Wenju Cai, editors, *El Niño Southern Oscillation in a Changing Climate*, pages 227–246. Wiley, first edition, November 2020.

[11] Ed Hawkins, Robin S. Smith, Jonathan M. Gregory, and David A. Stainforth. Irreducible uncertainty in near-term climate projections. *Climate Dynamics*, 46(11):3807–3819, June 2016.

[12] Nathan J. L. Lenssen, Lisa Goddard, and Simon Mason. Seasonal Forecast Skill of ENSO Teleconnection Maps. *Weather and Forecasting*, 35(6):2387–2406, December 2020.

[13] Lisa Goddard and Alexander Gershunov. Impact of El Niño on Weather and Climate Extremes. In *El Niño Southern Oscillation in a Changing Climate*, chapter 16, pages 361–375. American Geophysical Union (AGU), 2020.

[14] Weston Anderson, Richard Seager, Walter Baethgen, and Mark Cane. Life cycles of agriculturally relevant ENSO teleconnections in North and South America. *International Journal of Climatology*, 37(8):3297–3318, 2017.

[15] Bor-Ting Jong, Mingfang Ting, Richard Seager, and Weston B. Anderson. ENSO Teleconnections and Impacts on U.S. Summertime Temperature during a Multiyear La Niña Life Cycle. *Journal of Climate*, 33(14):6009–6024, July 2020.

[16] Mingfang Ting, Yochanan Kushnir, Richard Seager, and Cuihua Li. Forced and Internal Twentieth-Century SST Trends in the North Atlantic. *Journal of Climate*, 22(6):1469–1481, March 2009.

[17] Clara Deser, Michael A. Alexander, Shang-Ping Xie, and Adam S. Phillips. Sea Surface Temperature Variability: Patterns and Mechanisms. *Annual Review of Marine Science*, 2(1):115–143, 2010.

[18] Sumant Nigam, Bin Guan, and Alfredo Ruiz-Barradas. Key role of the Atlantic Multidecadal Oscillation in 20th century drought and wet periods over the Great Plains. *Geophysical Research Letters*, 38(16), 2011.

[19] Theodore G. Shepherd. Atmospheric circulation as a source of uncertainty in climate change projections. *Nature Geoscience*, 7(10):703–708, October 2014.

[20] Karen A. McKinnon and Clara Deser. Internal Variability and Regional Climate Trends in an Observational Large Ensemble. *Journal of Climate*, 31(17):6783–6802, September 2018.

[21] C. Deser, F. Lehner, K. B. Rodgers, T. Ault, T. L. Delworth, P. N. DiNezio, A. Fiore, C. Frankignoul, J. C. Fyfe, D. E. Horton, J. E. Kay, R. Knutti, N. S. Lovenduski, J. Marotzke, K. A. McKinnon, S. Minobe, J. Randerson, J. A. Screen, I. R. Simpson, and M. Ting. Insights from Earth system model initial-condition large ensembles and future prospects. *Nature Climate Change*, 10(4):277–286, April 2020.

[22] Laura Suarez-Gutierrez, Sebastian Milinski, and Nicola Maher. Exploiting large ensembles for a better yet simpler climate model evaluation. *Climate Dynamics*, 57(9):2557–2580, November 2021.

[23] Hannah Nissan, Lisa Goddard, Erin Coughlan de Perez, John Furlow, Walter Baethgen, Madeleine C. Thomson, and Simon J. Mason. On the use and misuse of climate change projections in international development. *WIREs Climate Change*, 10(3):e579, 2019.

[24] Stéphane Hallegatte. Strategies to adapt to an uncertain climate change. *Global Environmental Change*, 19(2):240–247, May 2009.

[25] Stéphane Hallegatte, Ankur Shah, Robert Lempert, Casey Brown, and Stuart Gill. *Investment Decision Making under Deep Uncertainty - Application to Climate Change*. Policy Research Working Papers. The World Bank, September 2012.

[26] Cristian Proistosescu and Gernot Wagner. Uncertainties in Climate and Weather Extremes Increase the Cost of Carbon. *One Earth*, 2(6):515–517, June 2020.

[27] Richard W. Katz and Barbara G. Brown. Extreme events in a changing climate: Variability is more important than averages. *Climatic Change*, 21(3):289–302, July 1992.

[28] Richard L. Revesz, Peter H. Howard, Kenneth Arrow, Lawrence H. Goulder, Robert E. Kopp, Michael A. Livermore, Michael Oppenheimer, and Thomas Sterner. Global warming: Improve economic models of climate change. *Nature*, 508(7495):173–175, April 2014.

[29] Franziska Piontek, Laurent Drouet, Johannes Emmerling, Tom Kompas, Aurélie Méjean, Christian Otto, James Rising, Bjoern Soergel, Nicolas Taconet, and Massimo Tavoni. Integrated perspective on translating biophysical to economic impacts of climate change. *Nature Climate Change*, 11(7):563–572, July 2021.

[30] Amy Dale, Charles Fant, Kenneth Strzepek, Megan Lickley, and Susan Solomon. Climate model uncertainty in impact assessments for agriculture: A multi-ensemble case study on maize in sub-Saharan Africa. *Earth's Future*, 5(3):337–353, 2017.

[31] Budong Qian, Qi Jing, Ward Smith, Brian Grant, Alex J. Cannon, and Xuebin Zhang. Quantifying the uncertainty introduced by internal climate variability in projections of Canadian crop production. *Environmental Research Letters*, 15(7):074032, July 2020.

[32] Olivier Deschênes and Michael Greenstone. Climate Change, Mortality, and Adaptation: Evidence from Annual Fluctuations in Weather in the US. *American Economic Journal: Applied Economics*, 3(4):152–185, October 2011.

[33] Tatyana Deryugina and Solomon M. Hsiang. Does the Environment Still Matter? Daily Temperature and Income in the United States. Working Paper 20750, National Bureau of Economic Research, December 2014.

[34] Wolfram Schlenker and Michael J. Roberts. Nonlinear temperature effects indicate severe damages to U.S. crop yields under climate change. *Proceedings of the National Academy of Sciences*, 106(37):15594–15598, September 2009.

[35] Matz A. Haugen, Michael L. Stein, Elisabeth J. Moyer, and Ryan L. Sriver. Estimating Changes in Temperature Distributions in a Large Ensemble of Climate Simulations Using Quantile Regression. *Journal of Climate*, 31(20):8573–8588, October 2018.

[36] Matz A. Haugen, Michael L. Stein, Ryan L. Sriver, and Elisabeth J. Moyer. Future climate emulations using quantile regressions on large ensembles. *Advances in Statistical Climatology, Meteorology and Oceanography*, 5(1):37–55, April 2019.

[37] Detlef P. van Vuuren, Jae Edmonds, Mikiko Kainuma, Keywan Riahi, Allison Thomson, Kathy Hibbard, George C. Hurtt, Tom Kram, Volker Krey, Jean-Francois Lamarque, Toshihiko Masui, Malte Meinshausen, Nebojsa Nakicenovic, Steven J. Smith, and Steven K. Rose. The representative concentration pathways: An overview. *Climatic Change*, 109(1-2):5, November 2011.

[38] Flavio Lehner, Clara Deser, Nicola Maher, Jochem Marotzke, Erich M. Fischer, Lukas Brunner, Reto Knutti, and Ed Hawkins. Partitioning climate projection uncertainty with multiple large ensembles and CMIP5/6. *Earth System Dynamics*, 11(2):491–508, May 2020.

[39] Nicola Maher, Flavio Lehner, and Jochem Marotzke. Quantifying the role of internal variability in the temperature we expect to observe in the coming decades. *Environmental Research Letters*, 15(5):054014, May 2020.

[40] Laura Suarez-Gutierrez, Nicola Maher, and Sebastian Milinski. Evaluating the internal variability and forced response in Large Ensembles. *US CLIVAR Variations*, 18:27–35, 2020.

[41] Centers for Disease Control and Prevention, National Center for Health Statistics. National Vital Statistics System, Mortality 1999-2020 on CDC WONDER Online Database. Data are from the Multiple Cause of Death Files, 1999-2020, as compiled from data provided by the 57 vital statistics jurisdictions through the Vital Statistics Cooperative Program., 2021.

[42] S. C. Sherwood, M. J. Webb, J. D. Annan, K. C. Armour, P. M. Forster, J. C. Hargreaves, G. Hegerl, S. A. Klein, K. D. Marvel, E. J. Rohling, M. Watanabe, T. Andrews, P. Braconnot, C. S. Bretherton, G. L. Foster, Z. Hausfather, A. S. von der Heydt, R. Knutti, T. Mauritsen, J. R. Norris, C. Proistosescu, M. Rugenstein, G. A. Schmidt, K. B. Tokarska, and M. D. Zelinka. An Assessment of Earth's Climate Sensitivity Using Multiple Lines of Evidence. *Reviews of Geophysics*, 58(4):e2019RG000678, 2020.

[43] Sebastian Milinski, Nicola Maher, and Dirk Olonscheck. How large does a large ensemble need to be? *Earth System Dynamics*, 11(4):885–901, October 2020.

[44] Aiguo Dai and Christine E. Bloecker. Impacts of internal variability on temperature and precipitation trends in large ensemble simulations by two climate models. *Climate Dynamics*, 52(1):289–306, January 2019.

[45] Raul R Wood, Flavio Lehner, Angeline G Pendergrass, and Sarah Schlunegger. Changes in precipitation variability across time scales in multiple global climate model large ensembles. *Environmental Research Letters*, 16(8):084022, August 2021.

[46] Karl E. Taylor, Ronald J. Stouffer, and Gerald A. Meehl. An Overview of CMIP5 and the Experiment Design. *Bulletin of the American Meteorological Society*, 93(4):485–498, October 2011.

[47] Paul Berrisford, D. Dee, K. Fielding, M. Fuentes, P. Kallberg, S. Kobayashi, and S. Uppala. The ERA-Interim Archive. Report 1, European Centre for Medium-Range Weather Forecasts, Shinfield Park, Reading, August 2009.

[48] Ed Hawkins, Thomas M. Osborne, Chun Kit Ho, and Andrew J. Challinor. Calibration and bias correction of climate projections for crop modelling: An idealised case study over Europe. *Agricultural and Forest Meteorology*, 170:19–31, March 2013.

[49] Jacqueline Diaz-Nieto and Robert L. Wilby. A comparison of statistical downscaling and climate change factor methods: Impacts on low flows in the River Thames, United Kingdom. *Climatic Change*, 69(2):245–268, April 2005.

[50] National Cancer Institute. Surveillance, Epidemiology, and End Results (SEER) Program Populations (1969-2019), February 2021.

[51] U.S. Bureau of Economic Analysis. CAGDP1 Gross Domestic Product (GDP) summary by county and metropolitan area, 2021.

[52] USDA NASS. 1979-2010 NASS Corn Yields, 2019.

[53] Megan C. Kirchmeier-Young, Francis W. Zwiers, and Nathan P. Gillett. Attribution of Extreme Events in Arctic Sea Ice Extent. *Journal of Climate*, 30(2):553–571, January 2017.

[54] S Jeffrey, L Rotstayn, M Collier, S Dravitzki, C Hamalainen, C Moeseneder, K Wong, and J Skytus. Australia's CMIP5 submission using the CSIRO-Mk3.6 model. *Australian Meteorological and Oceanographic Journal*, 63(1):1–14, March 2013.

[55] Nicola Maher, Sebastian Milinski, Laura Suarez-Gutierrez, Michael Botzet, Mikhail Dobrynin, Luis Kornblueh, Jürgen Kröger, Yohei Takano, Rohit Ghosh, Christopher Hedemann, Chao Li, Hongmei Li, Elisa Manzini, Dirk Notz, Dian Putrasahan, Lena Boysen, Martin Claussen, Tatiana Ilyina, Dirk Olonscheck, Thomas Raddatz, Bjorn Stevens, and Jochem Marotzke. The Max Planck Institute Grand Ensemble: Enabling the Exploration of Climate System Variability. *Journal of Advances in Modeling Earth Systems*, 11(7):2050–2069, 2019.

[56] Lantao Sun, Michael Alexander, and Clara Deser. Evolution of the Global Coupled Climate Response to Arctic Sea Ice Loss during 1990–2090 and Its Contribution to Climate Change. *Journal of Climate*, 31(19):7823–7843, October 2018.

[57] K. B. Rodgers, J. Lin, and T. L. Frölicher. Emergence of multiple ocean ecosystem drivers in a large ensemble suite with an Earth system model. *Biogeosciences*, 12(11):3301–3320, June 2015.

[58] J. E. Kay, C. Deser, A. Phillips, A. Mai, C. Hannay, G. Strand, J. M. Arblaster, S. C. Bates, G. Danabasoglu, J. Edwards, M. Holland, P. Kushner, J.-F. Lamarque, D. Lawrence, K. Lindsay, A. Middleton, E. Munoz, R. Neale, K. Oleson, L. Polvani, and M. Vertenstein. The Community Earth System Model (CESM) Large Ensemble Project: A Community Resource for Studying Climate Change in the Presence of Internal Climate Variability. *Bulletin of the American Meteorological Society*, 96(8):1333–1349, November 2014.

[59] Benjamin M. Sanderson, Keith W. Oleson, Warren G. Strand, Flavio Lehner, and Brian C. O'Neill. A new ensemble of GCM simulations to assess avoided impacts in a climate mitigation scenario. *Climatic Change*, 146(3):303–318, February 2018.

[60] Wilco Hazeleger, Camiel Severijns, Tido Semmler, Simona Ştefănescu, Shuting Yang, Xueli Wang, Klaus Wyser, Emanuel Dutra, José M. Baldasano, Richard Bintanja, Philippe Bougeault, Rodrigo Caballero, Annica M. L. Ekman, Jens H. Christensen, Bart van den Hurk, Pedro Jimenez, Colin Jones, Per Kållberg, Torben Koenigk, Ray McGrath, Pedro Miranda, Twan van Noije, Tim Palmer, José A. Parodi, Torben Schmith, Frank Selten, Trude Storelvmo, Andreas Sterl, Honoré Tapamo, Martin Vancoppenolle, Pedro Viterbo, and Ulrika Willén. EC-Earth: A Seamless Earth-System Prediction Approach in Action. *Bulletin of the American Meteorological Society*, 91(10):1357–1364, October 2010.

[61] Femke J. M. M. Nijsse, Peter M. Cox, and Mark S. Williamson. Emergent constraints on transient climate response (TCR) and equilibrium climate sensitivity (ECS) from historical warming in CMIP5 and CMIP6 models. *Earth System Dynamics*, 11(3):737–750, August 2020.

[62] Leo J. Donner, Bruce L. Wyman, Richard S. Hemler, Larry W. Horowitz, Yi Ming, Ming Zhao, Jean-Christophe Golaz, Paul Ginoux, S.-J. Lin, M. Daniel Schwarzkopf, John Austin, Ghassan Alaka, William F. Cooke, Thomas L. Delworth, Stuart M. Freidenreich, C. T. Gordon, Stephen M. Griffies, Isaac M. Held, William J. Hurlin, Stephen A. Klein, Thomas R. Knutson, Amy R. Langenhorst, Hyun-Chul Lee, Yanluan Lin, Brian I. Magi, Sergey L. Malyshev, P. C. D. Milly, Vaishali Naik, Mary J. Nath, Robert Pincus, Jeffrey J. Ploshay, V. Ramaswamy, Charles J. Seman, Elena Shevliakova, Joseph J. Sirutis, William F. Stern, Ronald J. Stouffer, R. John Wilson, Michael Winton, Andrew T. Wittenberg, and Fanrong Zeng. The Dynamical Core, Physical Parameterizations, and Basic Simulation Characteristics of the Atmospheric Component AM3 of the GFDL Global Coupled Model CM3. *Journal of Climate*, 24(13):3484–3519, July 2011.

[63] John P. Dunne, Jasmin G. John, Alistair J. Adcroft, Stephen M. Griffies, Robert W. Hallberg, Elena Shevliakova, Ronald J. Stouffer, William Cooke, Krista A. Dunne, Matthew J. Harrison, John P. Krasting, Sergey L. Malyshev, P. C. D. Milly, Peter J. Phillipps, Lori T. Sentman, Bonita L. Samuels, Michael J. Spelman, Michael Winton, Andrew T. Wittenberg, and Niki Zadeh. GFDL's ESM2 Global Coupled Climate–Carbon Earth System Models.

Part I: Physical Formulation and Baseline Simulation Characteristics. *Journal of Climate*, 25(19):6646–6665, October 2012.

[64] John P. Dunne, Jasmin G. John, Elena Shevliakova, Ronald J. Stouffer, John P. Krasting, Sergey L. Malyshev, P. C. D. Milly, Lori T. Sentman, Alistair J. Adcroft, William Cooke, Krista A. Dunne, Stephen M. Griffies, Robert W. Hallberg, Matthew J. Harrison, Hiram Levy, Andrew T. Wittenberg, Peter J. Phillips, and Niki Zadeh. GFDL's ESM2 Global Coupled Climate–Carbon Earth System Models. Part II: Carbon System Formulation and Baseline Simulation Characteristics*. *Journal of Climate*, 26(7):2247–2267, April 2013.

[65] Gavin A. Schmidt, Max Kelley, Larissa Nazarenko, Reto Ruedy, Gary L. Russell, Igor Aleinov, Mike Bauer, Susanne E. Bauer, Maharaj K. Bhat, Rainer Bleck, Vittorio Canuto, Yong-Hua Chen, Ye Cheng, Thomas L. Clune, Anthony Del Genio, Rosalinda de Fainchtein, Greg Faluvegi, James E. Hansen, Richard J. Healy, Nancy Y. Kiang, Dorothy Koch, Andy A. Lacis, Allegra N. LeGrande, Jean Lerner, Ken K. Lo, Elaine E. Matthews, Surabi Menon, Ron L. Miller, Valdar Oinas, Amidu O. Oloso, Jan P. Perlwitz, Michael J. Puma, William M. Putman, David Rind, Anastasia Romanou, Makiko Sato, Drew T. Shindell, Shan Sun, Rahman A. Syed, Nick Tausnev, Kostas Tsigaridis, Nadine Unger, Apostolos Voulgarakis, Mao-Sung Yao, and Jinlun Zhang. Configuration and assessment of the GISS ModelE2 contributions to the CMIP5 archive. *Journal of Advances in Modeling Earth Systems*, 6(1):141–184, 2014.

[66] G.M. Martin, N. Bellouin, W. J. Collins, I. D. Culverwell, P. R. Halloran, S. C. Hardiman, T. J. Hinton, C. D. Jones, R. E. McDonald, A. J. McLaren, F. M. O'Connor, M. J. Roberts, J. M. Rodriguez, S. Woodward, M. J. Best, M. E. Brooks, A. R. Brown, N. Butchart, C. Dearden, S. H. Derbyshire, I. Dharssi, M. Doutriaux-Boucher, J. M. Edwards, P. D. Falloon, N. Gedney, L. J. Gray, H. T. Hewitt, M. Hobson, M. R. Huddleston, J. Hughes, S. Ineson, W. J. Ingram, P. M. James, T. C. Johns, C. E. Johnson, A. Jones, C. P. Jones, M. M. Joshi, A. B. Keen, S. Liddicoat, A. P. Lock, A. V. Maidens, J. C. Manners, S. F. Milton, J. G. L. Rae, J. K. Ridley, A. Sellar, C. A. Senior, I. J. Totterdell, A. Verhoef, P. L. Vidale, and A. Wiltshire. The HadGEM2 family of Met Office Unified Model climate configurations. *Geoscientific Model Development*, 4(3):723–757, September 2011.

[67] J.-L. Dufresne, M.-A. Foujols, S. Denvil, A. Caubel, O. Marti, O. Aumont, Y. Balkanski, S. Bekki, H. Bellenger, R. Benshila, S. Bony, L. Bopp, P. Braconnot, P. Brockmann, P. Cadule, F. Cheruy, F. Codron, A. Cozic, D. Cugnet, N. de Noblet, J.-P. Duvel, C. Ethé, L. Fairhead, T. Fichefet, S. Flavoni, P. Friedlingstein, J.-Y. Grandpeix, L. Guez, E. Guilyardi, D. Hauglustaine, F. Hourdin, A. Idelkadi, J. Ghattas, S. Joussaume, M. Kageyama, G. Krinner, S. Labetoulle, A. Lahellec, M.-P. Lefebvre, F. Lefevre, C. Levy, Z. X. Li, J. Lloyd, F. Lott, G. Madec, M. Mancip, M. Marchand, S. Masson, Y. Meurdesoif, J. Mignot, I. Musat, S. Parouty, J. Polcher, C. Rio, M. Schulz, D. Swingedouw, S. Szopa, C. Talandier, P. Terray, N. Viovy, and N. Vuichard. Climate change projections using the IPSL-CM5 Earth System Model: From CMIP3 to CMIP5. *Climate Dynamics*, 40(9-10):2123–2165, May 2013.

[68] S. Watanabe, T. Hajima, K. Sudo, T. Nagashima, T. Takemura, H. Okajima, T. Nozawa, H. Kawase, M. Abe, T. Yokohata, T. Ise, H. Sato, E. Kato, K. Takata, S. Emori, and M. Kawamiya. MIROC-ESM 2010: Model description and basic results of CMIP5-20c3m experiments. *Geoscientific Model Development*, 4(4):845–872, October 2011.

[69] Masahiro Watanabe, Tatsuo Suzuki, Ryouta O'ishi, Yoshiki Komuro, Shingo Watanabe, Seita Emori, Toshihiko Takemura, Minoru Chikira, Tomoo Ogura, Miho Sekiguchi, Kumiko Takata, Dai Yamazaki, Tokuta Yokohata, Toru Nozawa, Hiroyasu Hasumi, Hiroaki Tatebe, and Masahide Kimoto. Improved Climate Simulation by MIROC5: Mean States, Variability, and Climate Sensitivity. *Journal of Climate*, 23(23):6312–6335, December 2010.

[70] Seiji Yukimoto, Yukimasa Adachi, Masahiro Hosaka, Tomonori Sakami, Hiromasa Yoshimura, Mikitoshi Hirabara, Taichu Y. Tanaka, Eiki Shindo, Hiroyuki Tsujino, Makoto Deushi, Ryo Mizuta, Shoukichi Yabu, Atsushi Obata, Hideyuki Nakano, Tsuyoshi Koshiro, Tomoaki Ose, and Akio Kitoh. A New Global Climate Model of the Meteorological Research Institute: MRI-CGCM3 —Model Description and Basic Performance—. *Journal of the Meteorological Society of Japan. Ser. II*, 90A:23–64, 2012.

[71] M. Bentsen, I. Bethke, J. B. Debernard, T. Iversen, A. Kirkevåg, Ø Seland, H. Drange, C. Roelandt, I. A. Seierstad, C. Hoose, and J. E. Kristjánsson. The Norwegian Earth System Model, NorESM1-M – Part 1: Description and basic evaluation of the physical climate. *Geoscientific Model Development*, 6(3):687–720, May 2013.

[72] T. Iversen, M. Bentsen, I. Bethke, J. B. Debernard, A. Kirkevåg, Ø Seland, H. Drange, J. E. Kristjansson, I. Medhaug, M. Sand, and I. A. Seierstad. The Norwegian Earth System Model, NorESM1-M – Part 2: Climate response and scenario projections. *Geoscientific Model Development*, 6(2):389–415, March 2013.

S1 Supplementary Figures

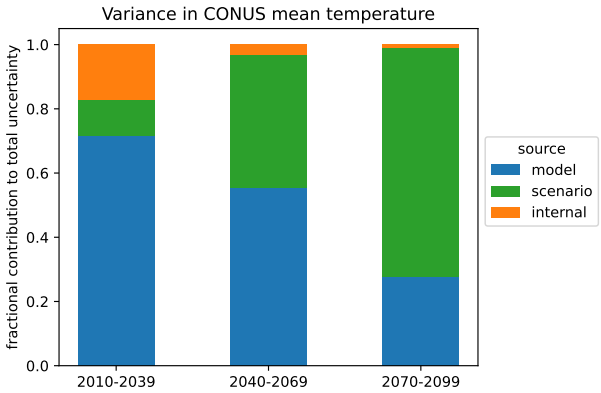

Figure S1: Partitioning of sources of uncertainty in projections of 30-year mean temperature over the CONUS. Figure constructed as in Figure 1i-k. Due to nonlinearities in dose-response functions, partitioning of climate uncertainty in impact projections is different from that in calculations of temperature alone.

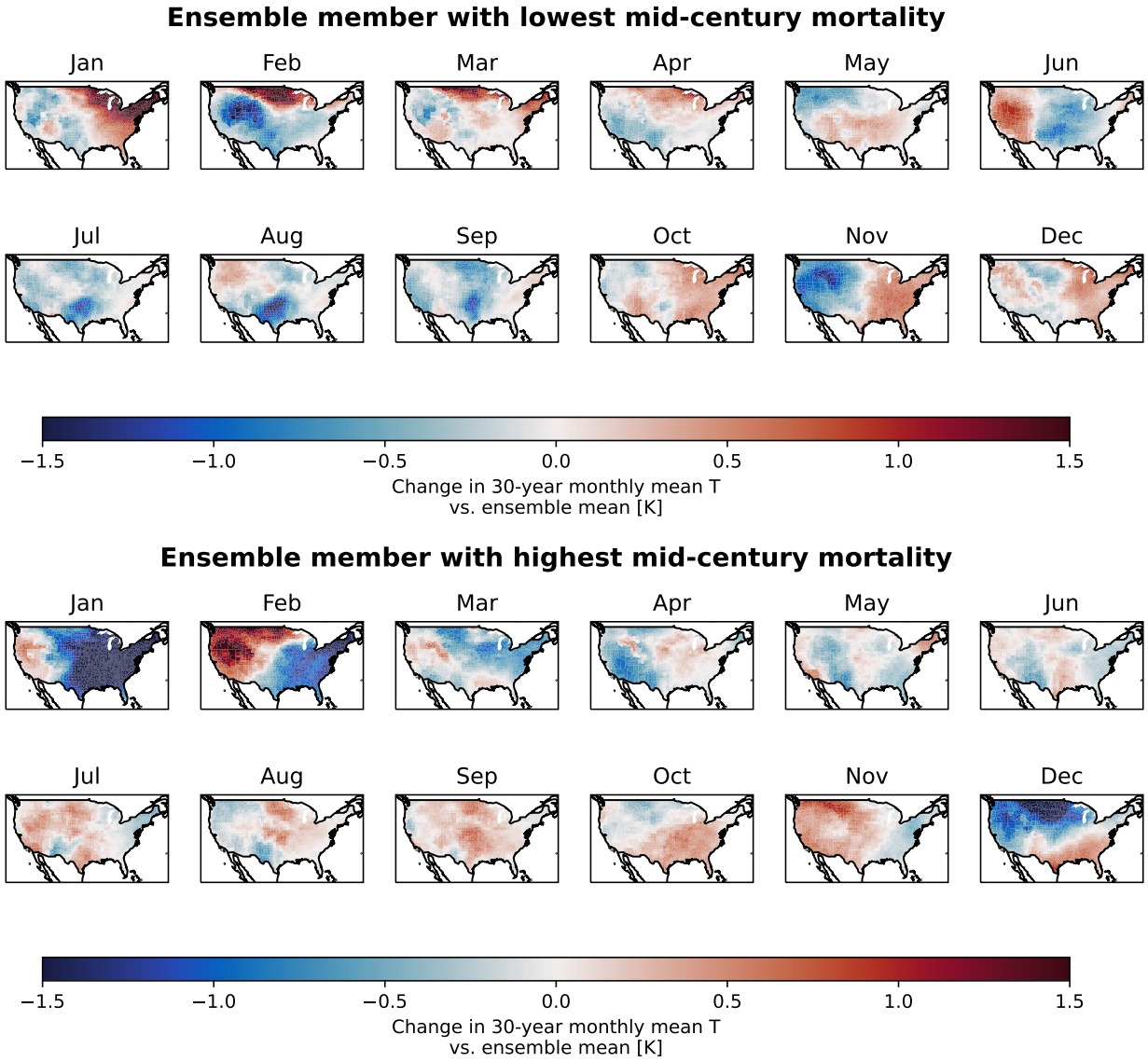

Figure S2: Relative change in monthly mean temperature vs. ensemble average for CESM1-CAM5 ensemble member projecting the lowest (top) and highest (bottom) mid-century mortality. The lowest mortality run has lower temperature increases in July than the average ensemble member, while the highest mortality run has the opposite, in addition to having less warming in January over much of CONUS.

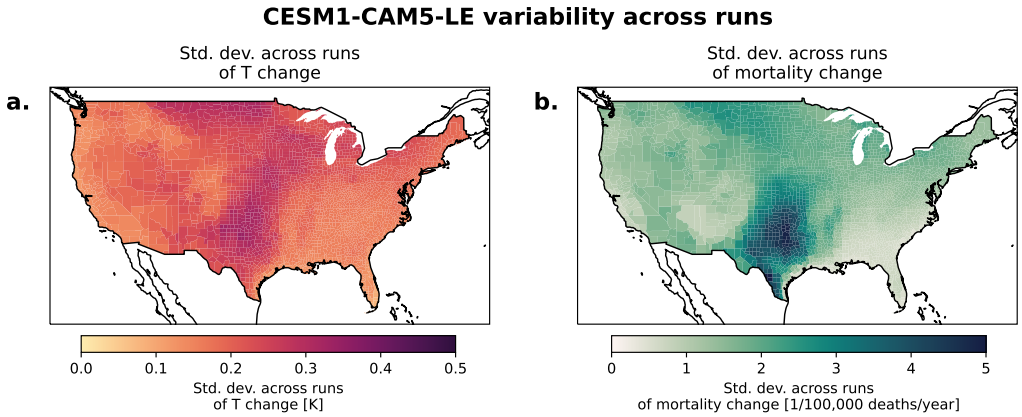

Figure S3: Geographic distribution of variability across runs in mean temperature change and projected mortality rate change in CESM1-CAM5 in the mid-century period (2040-2069).

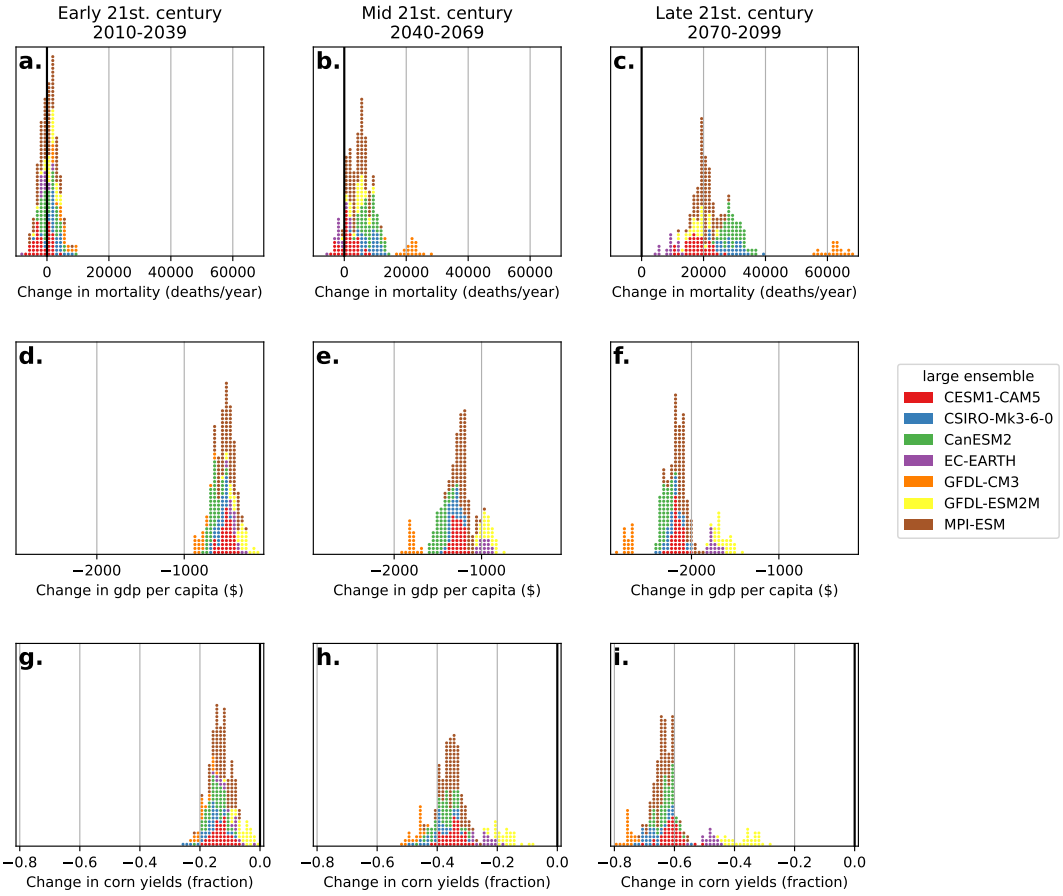

Figure S4: As Figure 3, but including all three examined impacts.

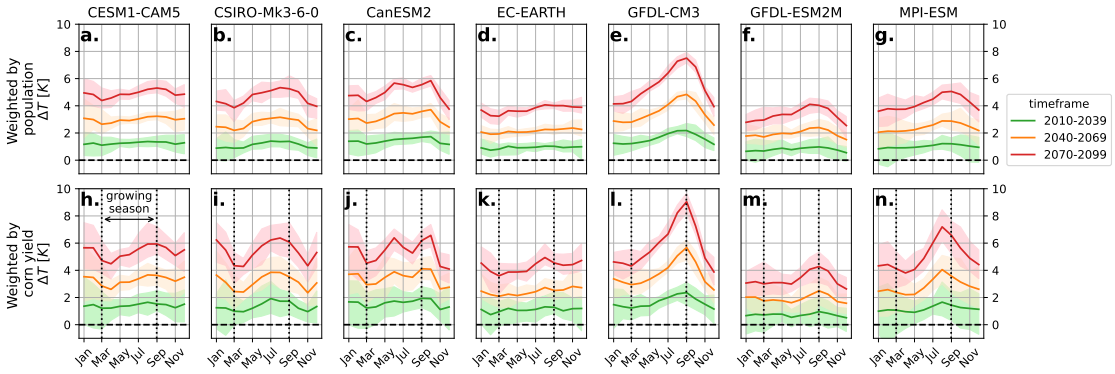

Figure S5: Change in mean CONUS temperature by month in models, showing changes in the seasonal cycle. Figure shows changes between the historical (1980-2009) period and 30 year periods in the early, mid, and late 21st century for each of the seven large ensembles where monthly temperature is (top row) weighted by population (bottom row) weighted by corn yield. The dotted vertical lines on the bottom row show the growing season, or months used in the corn yield impact study, from March to September. The shaded area spans the minimum and maximum ensemble member at each month.

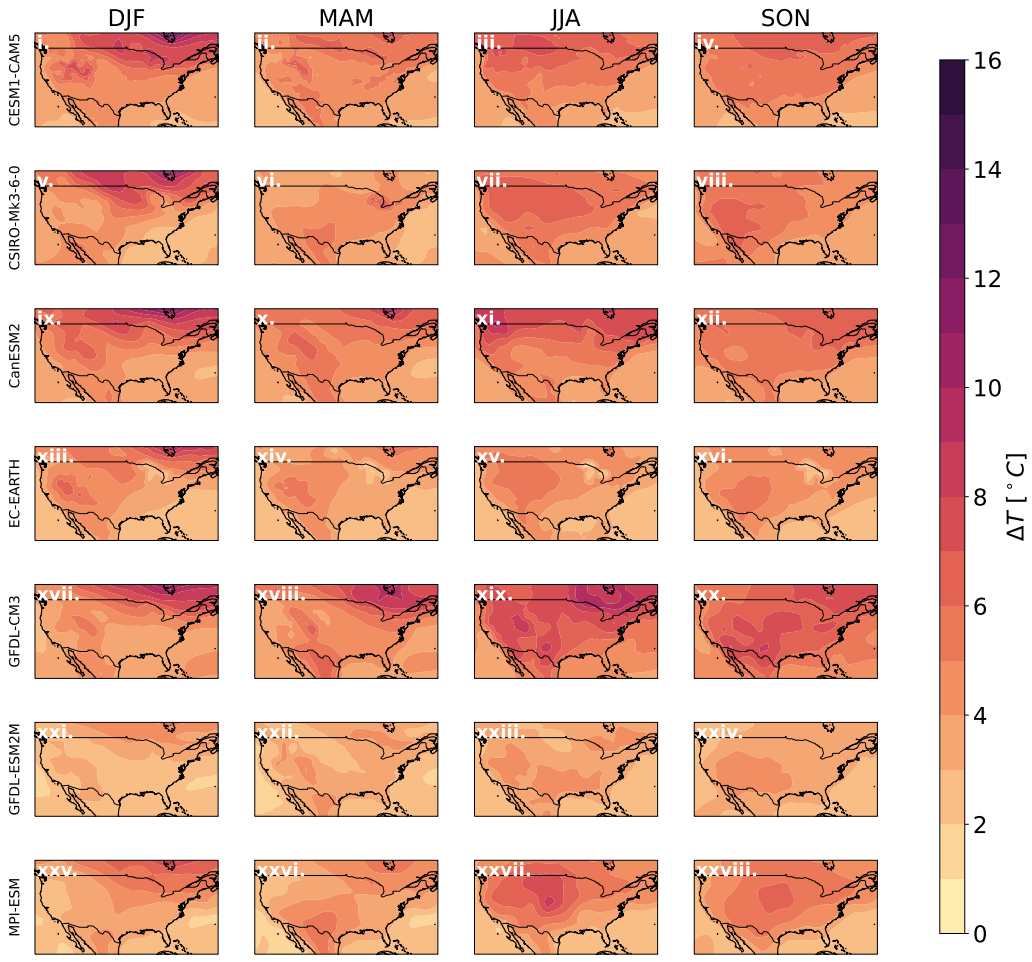

Figure S6: The spatial pattern of projected CONUS mean temperature change in 2070-2099 for each season, averaged across runs for each LE. Note particularly high warming during summer (JJA) and fall (SON) in GFDL-CM3 (panels xix.-xx.).

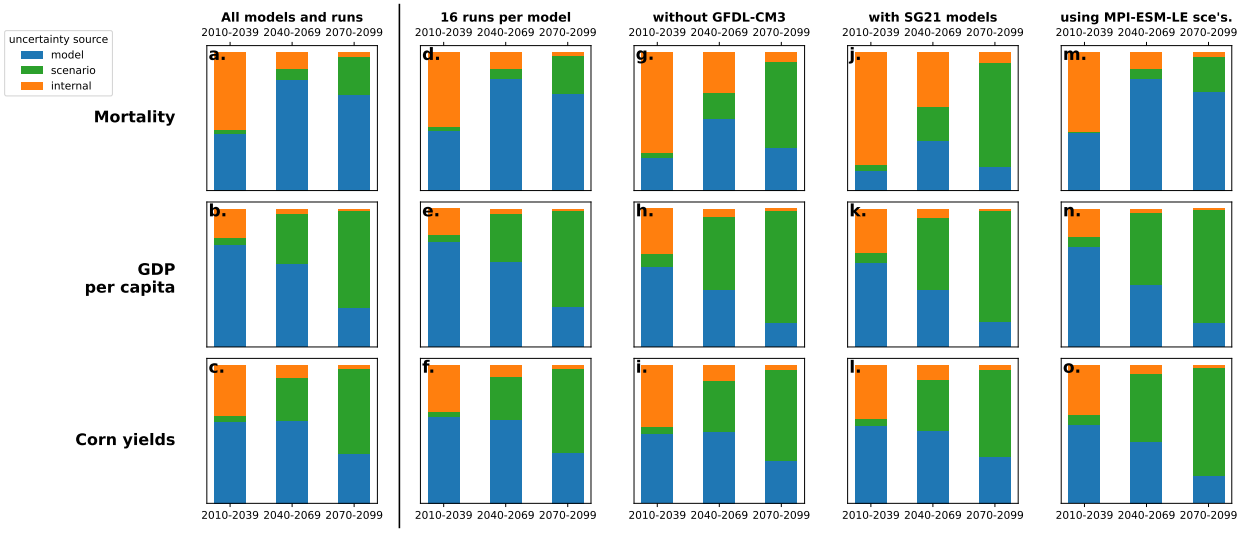

Figure S7: As Figure 1i.-k., but showing calculations using subsets of data. Panels a.-c. are identical to Figure 1i.-k. for reference; d.-f. were calculated using only 16 runs from each model (the number of runs from the smallest ensemble, EC-EARTH); g.-i. were calculated without runs from GFDL-CM3; j.-l. were calculated using the models found to best simulate internal variability and secular changes over CONUS by [40] (MPI-ESM, GFDL-ESM2M, CESM1-CAM5, CanESM2); m.-o. use the LE MPI-ESM to calculate scenario uncertainty instead of the selection of CMIP5 models. Note: the decreased relative importance of model uncertainty in panels j.-l. is likely due to [40] having subset models by closeness to a common target of observations.

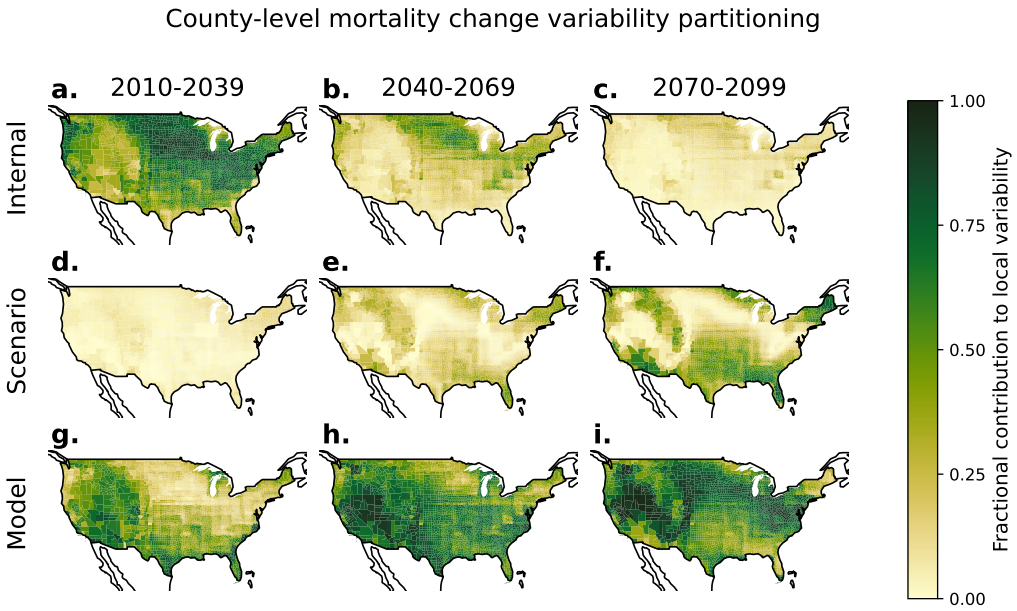

Figure S8: The partitioning of climate uncertainty in mortality projections at county level. These maps, as well as the maps shown in Figures S9 and S10 are synthesized in Figure 4 of the main text.

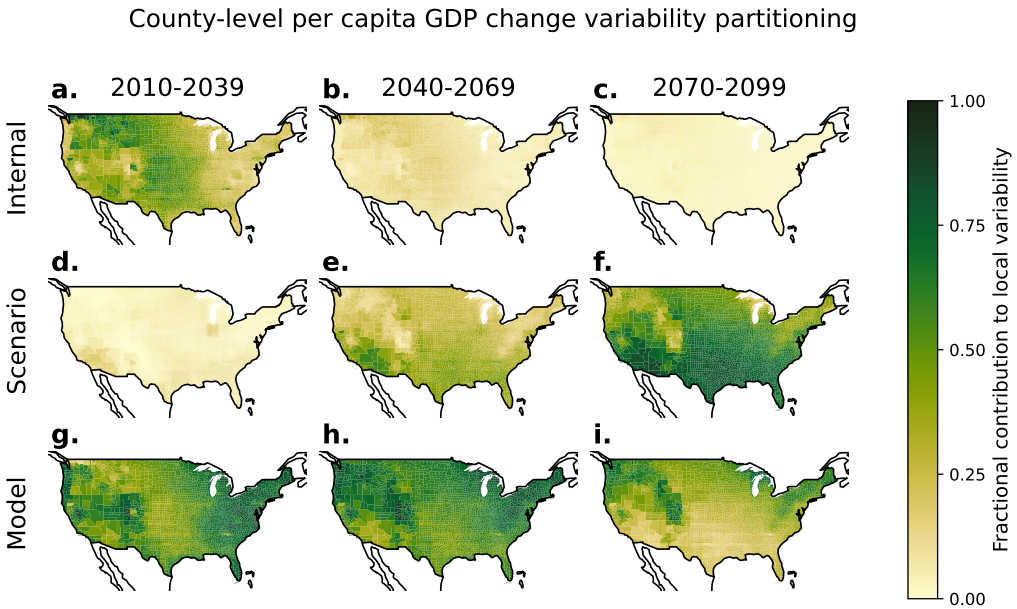

Figure S9: The partitioning of climate uncertainty in GDP projections at county level. These maps, as well as the maps shown in Figures S8 and S10 are synthesized in Figure 4 of the main text.

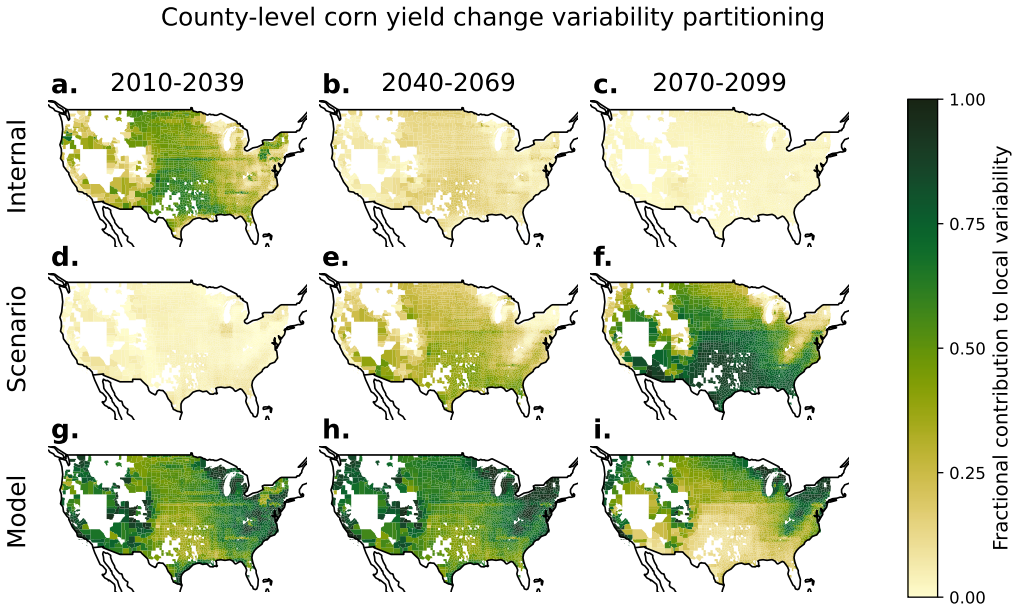

Figure S10: The partitioning of climate uncertainty in corn yield projections at county level. These maps, as well as the maps shown in Figures S8 and S9 are synthesized in Figure 4 of the main text. White areas show regions without corn production in the NASS dataset.

S2 Supplementary Tables

Table S1: Relative climate uncertainty in impact projections by source.

relative contribution to var		2010-2039	2040-2069	2070-2099
mortality	internal	0.56	0.12	0.03
	scenario	0.03	0.07	0.28
	model	0.41	0.80	0.69
per capita gdp	internal	0.20	0.04	0.01
	scenario	0.06	0.36	0.70
	model	0.74	0.60	0.28
corn yield	internal	0.37	0.09	0.03
	scenario	0.05	0.32	0.62
	model	0.59	0.59	0.36

Relative contribution by climate uncertainty to total outcome variance by source for the three time periods (columns) and three impact variables (rows) studied. Table shows values used in stacked bar charts in Figure 1 i.-k.

Table S2: Absolute climate uncertainty in impact projections by source.

absolute contribution to var		2010-2039	2040-2069	2070-2099
mortality (10^6 [deaths per year]^2)	internal	5.78	6.89	10.7
	scenario	0.29	4.20	101
	model	4.20	45.6	253
per capita gdp (10^4 \$^{2})	internal	0.50	0.45	0.50
	scenario	0.14	4.57	28.2
	model	1.82	7.53	11.3
corn yield $\left(10^{-3}\right)$	internal	0.99	1.22	1.05
	scenario	0.12	4.47	23.9
	model	1.59	8.37	13.9

Absolute contribution by climate uncertainty to total outcome variance by source for the three time periods (columns) and three impact variables (rows) studied. Table shows values used in stacked bar charts in Figure 1 l.-n.

Table S3: Large Ensemble output used.

Model	citation	# ensemble members	ECS	TCR
CanESM2	[53]	50	3.71	2.30
CSIRO-Mk3-6-0	[54]	30	4.36	1.69
MPI-ESM-LR	[55]	100	3.66	2.01
GFDL-CM3	[56]	30	4.03	1.76
GFDL-ESM2M	[57]	20	2.46	1.37
CESM1-CAM5	[58, 59]	40	-	2.29
EC-EARTH	[60]	16	-	-

Details of Large Ensemble used, with number of ensemble members, and ECS and TCR as given in the supplement of [61]. Models whose ECS values are outside of the 2.3-4.7 range may run counter to historical, paleoclimate, and theoretical understandings about the magnitude of climate change [42].

Table S4: CMIP5 models used to characterize scenario uncertainty.

Model	citation
CSIRO Mk3.6.0	[54]
GFDL-CM3	[62]
GFDL-ESM2G	[63, 64]
GFDL-ESM2M	[63, 64]
GISS-E2-H	[65]
GISS-E2-R	[65]
HadGEM2-AO	[66]
IPSL-CM5A-LR	[67]
IPSL-CM5A-MR	[67]
MIROC-ESM-CHEM	[68]
MIROC-ESM	[68]
MIROC5	[69]
MRI-CGCM3	[70]
NorESM1-M	[71, 72]